Carbonation of recycled concrete aggregate in a fixed-bed reactor: Effects of temperature, initial water saturation degree and particle size

Corvec Gaël, Riccardo Artoni, Philippe Turcry, Abdelkarim Aït-Mokhtar, Patrick Richard, Bogdan Cazacliu

Journal of CO2 Utilization 102 (2025) 103286

Contents lists available at ScienceDirect

Journal of CO2 Utilization

journal homepage: www.elsevier.com/locate/jcou

Carbonation of recycled concrete aggregate in a fixed-bed reactor: Effects of temperature, initial water saturation degree and particle size

CORVEC Gaël [a,b,*], ARTONI Riccardo [b], TURCRY Philippe [a], AIT-MOKHTAR Abdelkarim [a], RICHARD Patrick [b], CAZACLIU Bogdan [b]

[a] LaSIE, UMR CNRS 7556, La Rochelle Université, La Rochelle 17000, France
[b] Université Gustave Eiffel, MAST-GPEM, Bouguenais 44344, France

ARTICLE INFO

Keywords:
Recycled concrete aggregates
Carbonation
Carbon Capture and Utilization (CCU)
Temperature
Water saturation degree

ABSTRACT

Accelerated carbonation of recycled concrete aggregates (RCA) in industrial CO_2-rich environments is a promising technique to enhance CO_2 sequestration while improving RCA properties. This study investigates the influence of temperature (50–110 °C), initial water saturation degree (0.34–0.93), and RCA particle size (0–4 mm) on carbonation efficiency in a fixed-bed reactor under controlled conditions, simulating cement plant flue gases. Results highlight that water saturation degree is a key parameter, as it influences both CO_2 transport in the pore system and the dissolution of reactive phases. Temperature significantly impacts water saturation degree evolution, which in turn affects reaction kinetics. For each initial water saturation degree, an optimal temperature maximizes carbonation, reaching degrees above 40 % after only 2 h carbonation. Particle size also influences carbonation efficiency: finer RCA exhibit higher carbonation rates. A novel Macro-TGA methodology was employed to quantify carbonate formation in 500 g samples, offering a more representative assessment compared to classical thermogravimetric analyses. Finally, water absorption tests before and after carbonation showed a slight reduction, with a maximum decrease of 2.7 % at 80 °C and 0.93 initial water saturation degree. However, no direct correlation between water absorption and carbonation degree was observed, suggesting complex porosity evolution that requires further investigation.

1. Introduction

The production of cement is responsible for around 6 % of anthropogenic carbon dioxide (CO_2) emissions [1]. These greenhouse gas emissions result for 58 % from the high-temperature decarbonization reaction of calcium carbonate into calcium oxide and the rest corresponds to the combustion of fossil fuel and electricity use [2]. Through carbonation, cementitious materials can recapture part of the CO_2 released during their production, both during the service life of structures and after demolition [3]. Carbonation involves a series of physico-chemical mechanisms. Firstly, CO_2 diffuses through the pores of the material and dissolves in the water present on the surface of the reactive phases, notably portlandite ($Ca(OH)_2$) and calcium silicates hydrates (C-S-H). This dissolution leads to the formation of carbonate ions (CO_3^{2-}), which then precipitate as $CaCO_3$ by reacting with the dissolved calcium. Carbonation therefore corresponds to the mineralization of CO_2 in a thermodynamically stable manner.

Recycled concrete aggregates (RCA) are obtained by crushing demolition waste from concrete structures. RCA are mainly used in road construction and increasingly as a partial substitute of natural aggregates in concrete formulations. Carbonation of RCA is increasingly studied as it transforms construction waste into a carbon sink within the scope of Carbon Capture and Utilization (CCU) [4]. When using CO_2 from industrial sources, the carbon mineralized by RCA can potentially be monetized through emissions trading mechanisms such as ETS credits, thereby improving the economic viability of such sustainable recycling strategies [5]. Moreover, carbonation is suggested to improve the properties of RCA, particularly by reducing their water absorption [6]. Thus, carbonating RCA could enhance their recyclability while also sequestering CO_2 [5].

After crushing, RCA are stored several months in stockpiles. Hou et al. [7] have shown that the CO_2 uptake of the latter is very low. Only the skin of the stockpile can be carbonated in atmospheric conditions. Accelerated carbonation of RCA should be favored to take full advantage

* Corresponding author at: LaSIE, UMR CNRS 7556, La Rochelle Université, La Rochelle 17000, France.
E-mail addresses: gael.corvec@univ-lr.fr, gaelcorvec@orange.fr (C. Gaël).

https://doi.org/10.1016/j.jcou.2025.103286
Received 22 August 2025; Received in revised form 19 November 2025; Accepted 27 November 2025
Available online 29 November 2025

of their CO_2 binding capacity. Accelerated carbonation can be achieved through various approaches [8]. While some methods involve the extraction of reactive phases or the use of purified gases, these processes add complexity and energy consumption to a technique that offers few economic and environmental benefits [9,10]. Therefore, it seems more relevant to focus on direct carbonation of raw RCA using untreated industrial gases. While indirect carbonation are carried out exclusively in aqueous solution, direct methods can be performed under wet, semi-dry or dry conditions [8]. The semi-dry process is the focus of the present study. This kind of processes was previously investigated during the French national project FastCarb (2018–2022). The latter aimed to develop a process for carbonating RCA by CO_2-rich gas emitted by cement plants [10]. The project demonstrated the industrial feasibility of the process by using large-scale reactors. One of these demonstrators consisted of a fluidized RCA bed through which CO_2-rich gas from an exhaust stack flowed. The project highlighted the need to better understand the effect of temperature and water content of RCA on carbonation to improve the process efficiency. The flue gas emitted by cement plants can even exceed 160 °C [11] and has a water concentration of 7 % [12]. Temperature inside the large-scale RCA bed reactor of the FastCarb project reached 80 °C.

Temperature and water content of RCA have complex effects on various carbonation steps. A high-water saturation degree of RCA creates a wider environment in the pores where the reactants can meet for carbonation [13]. However, it also reduces the gaseous phase in the material and then slows down the penetration of CO_2 into the pores [14], as diffusion in water is 10,000 time slower in water than in air [15]. Thus, there is usually an optimum water content for carbonation [6,16]. Given the strong correlation between the water content of the cementitious materials and the water vapor content of the environment surrounding the material, there is also an optimum water vapor content maximizing carbonation [17–20].

Moisture content plays a central role in controlling carbonation mechanisms. By promoting pore drying, elevated temperatures alter these moisture conditions, thereby impacting the dissolution of reactive species and CO_2 transport [21,22]. Beyond moisture effects, temperature also alters the thermodynamic and kinetic parameters of the chemical reactions. On one hand, the solubility of key carbonation reactants such as portlandite, calcium silicate hydrates (C-S-H), and CO_2 decreases with rising temperature [23,24], potentially limiting their availability in solution and slowing down carbonation [26]. On the other hand, an increase in temperature accelerates transport processes such as gas diffusion [25], and ionic diffusion of reactants in the interstitial solution [26,27]. Furthermore, the lower solubility of calcite (the main reaction product) at higher temperatures promotes its precipitation [28], which favors the overall carbonation process. The net effect of temperature therefore results from the interplay between improved mass transport, modified moisture conditions, and changes in solubility of both reactants and products. Several studies [17,19,21] investigated the effect of the temperature on carbonation in reinforced concrete structures by evaluating the progression of the carbonation front in the range of 20 °C to 80 °C. These studies have shown that higher temperatures increase the carbonation rate, which can reduce the service life of reinforced concrete. Other works [6,29–31] have examined the use of carbonation to sequester CO_2 in cement-based materials. In this context, the assessment of carbonation is based on the total amount of sequestered CO_2 rather than the depth of the reaction front. These studies, conducted at temperatures between 5 °C and 70 °C, also reported an increase in carbonation with temperature. When studying higher temperatures (up to 300 °C) [16,20,32–34], an optimal temperature range between 60 and 100 °C was found for a faster carbonation. Carbonation of a cement paste powder in aqueous solution is also slightly improved by temperature from 20 to 80 °C [35,36].

The use of industrial flue gases for accelerated carbonation is particularly appealing, as these gases are hot and contain water vapor. Such conditions can potentially enhance carbonation reaction. Previous studies on industrial processes have examined the carbonation of RCA in fluidized beds or rotary drum reactors [10,37], which enable continuous operation and efficient gas–solid contact. However, these configurations make it difficult to independently control temperature and moisture within the reactive bed and to isolate their respective effects. The carbonation of RCA in a fixed-bed reactor has not yet been studied to our knowledge. This type of reactor offers a simplified but representative system for fundamental investigations. To better understand and optimize these operating conditions before industrial implementation, the present study was conducted at the laboratory scale using a fixed-bed reactor, which enables precise control of temperature and water content of RCA and allows parametric investigation of their combined effects on process efficiency. In this study, the influence of temperature (50–110 °C) and initial water saturation degree (0.34 – 0.93) on the CO_2 uptake was investigated in a fixed-bed reactor, through which a gas stream with a composition aiming to model a cement plant flue gas was flowed. Two innovative methods were used to quantify the amount of bound CO_2: a large-scale thermogravimetric analysis (named Macro-TGA in the following) presented in details in [38] and an indirect gas analysis at the reactor outlet. The effect of particle size on carbonation efficiency was also investigated. The temperature and initial water saturation degree were studied simultaneously to assess their combined impact. The reaction time was fixed at 2 h. This study investigates these two key-parameters influencing RCA carbonation, with the aim of supporting the optimization of large-scale industrial devices.

2. Materials and methods

The overall experimental procedure used to study the carbonation of RCA is summarized in Fig. 1. It includes the preparation of the materials, carbonation setup, and the different characterization steps before and after carbonation. Each stage is detailed in the following subsections.

2.1. Studied materials and preparation

In this study, tests were performed on a “model” RCA. It was obtained from a cast mortar to ensure a homogeneous RCA composition. The cement used is an ordinary Portland cement (CEM I 52.5 R) from Calcia (Ranville factory, France). Its chemical composition is given in Table 1. The siliceous alluvial sand (0/2 mm from Lafarge Vritz factory, France) does not contain calcium carbonate, thereby preventing interference in the quantification of carbonation.

The water/cement mass ratio used was 0.5 and the sand/cement mass ratio of 2.16 (with this ratio, the volume fraction of sand is 0.5). The mortar was cast in slab form of 1.6 m^2 and 3.5 cm thickness. After 24 h, the slab was broken into small pieces (maximal width < 20 cm) while the material was still sufficiently weak to be fragmented without excessive mechanical effort. The maximal width was chosen to provide pieces of suitable dimensions for the subsequent jaw-crushing stage. Immediately after obtaining, the small pieces were immersed in a water tank for at least 2 months to ensure complete hydration and to protect the material from carbonation during this storage phase. Finally, after water conservation, the mortar pieces were crushed with a laboratory jaw crusher to obtain aggregates in the 0/4 mm size range. A sample of RCA was characterized before accelerated carbonation as a reference (RCA-NC) to determine the particle size distribution, initial CO_2 content and initial water absorption. The particle size distribution is shown in Fig. 2.

To study the effect of the initial water saturation degree on carbonation, RCA samples were either partially or almost fully saturated with water. In this study, the water saturation degree refers to the ratio between the actual water content of RCA, w [%], and its total water absorption, A [%]:

$$S = w/A \quad (1)$$

S ranges from 0 (dry state at 60 °C) to 1 (full water absorption). It

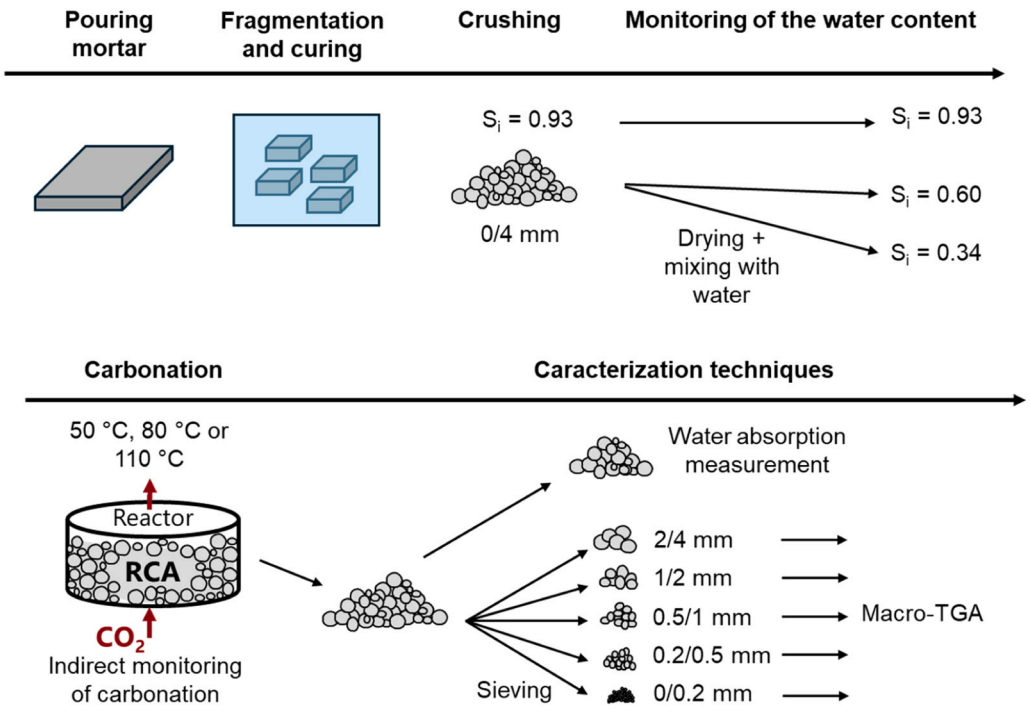

Fig. 1. Overview of the experimental workflow from material preparation and carbonation process to characterization techniques.

Table 1
Chemical composition of the Portland cement used.

Composition	Mass %
CaO	63.5
SiO_2	19.8
Al_2O_3	4.7
Fe_2O_3	3.9
MgO	1.1
Na_2O	0.05
K_2O	0.86
SO_3	3.5
Loss of ignition (LOI)	2.5

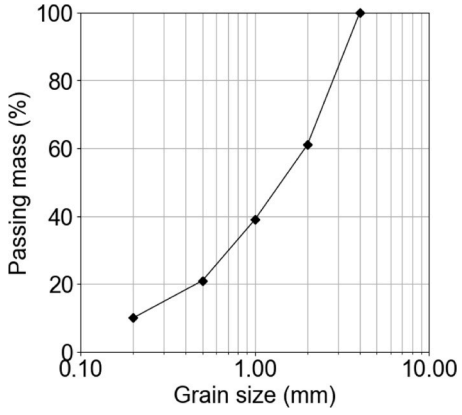

Fig. 2. Particle size distribution for the non-carbonated material obtained after just after crushing (RCA-NC).

therefore characterizes the internal moisture of the material rather than the ambient relative humidity (RH), although both parameters are physically related through vapor–liquid equilibrium. RCA samples were prepared with three different water saturation degrees following the protocols below.

Partially water-saturated RCA (S = 0.34 and 0.60) were prepared by oven-drying RCA at 60 °C until constant mass (mass variation < 0.05 % during 24 h), then mixing with the required amount of water in sealed plastic bags. The mixture was homogenized and stored between 7 and 20 days before use. The reference dry mass was chosen as the mass of the oven-dried sample at 60 °C. The latter temperature was chosen to prevent the chemical dehydration of water bound to hydrates, such as C-S-H and ettringite which can occur at higher temperature [39].

After curing and crushing, the studied RCA were considered almost fully water-saturated. Samples were stored in sealed plastic bags for a maximum of 12 days before testing. The initial mass at 60 °C of these saturated samples, $m^i_{60°C}$ [g], was not directly measured, as this would have required drying the samples and thus altering their initial saturation state. Instead, it was estimated indirectly, assuming that the mass at 950 °C remains constant regardless of water saturation or carbonation state. The estimation of $m^i_{60°C}$ was based on the final dried mass after carbonation ($m^f_{60°C}$ [g]), the mass ratio at 60 °C and 950 °C of the non-carbonated sample ($R^{NC}_{60°C/950°C} = 1.075$), determined with Macro-TGA (Sections 2–6), and the mass ratio after carbonation $R^{C}_{60°C/950°C}$ using the following relationship:

$$m^i_{60°C} = \frac{m^f_{60°C} R^{NC}_{60°C/950°C}}{R^{C}_{60°C/950°C}} \quad (2)$$

This estimated mass was then used to determine the initial water saturation degree of the saturated samples depending on the water absorption determined with the method described in Section 2.7. The calculated values were approximately 0.94 for the samples tested at 50 °C, 0.97 at 80 °C, and 0.88 at 110 °C. For simplicity, all the samples that are nearly water-saturated are referred to by the average water saturation degree of all these samples, i.e., 0.93, in the following.

A total of nine carbonation tests were conducted for 120 min, covering the nine combinations of water saturation degree and temperature listed in Table 2. In addition, one test was performed over 15 min at 80 °C with 0.93 saturated sample. The temperature range (50–110 °C) was selected to prevent water condensation from the gas mixture (Section 2.2) while remaining representative of the gas

Table 2
Experimental plan with the parameter combinations tested.

Carbonation time (min)	Temperature (°C)	Initial water saturation degree
120	50	0.34 – 0.60 – 0.93
120	80	0.34 – 0.60 – 0.93
120	110	0.34 – 0.60 – 0.93
15	80	0.93

temperatures expected in industrial carbonation demonstrators, where RCA are exposed to hot flue gases, as discussed in the Introduction. The upper limit was kept below 110 °C for technical reasons.

2.2. Gas preparation

To simulate industrial flue gas conditions, carbonation was carried out using a "model" gas mixture. This gas was designed to reflect the composition of typical emissions from cement plants, which are characterized by a water vapor pressure of approximately 7 kPa and a CO_2 concentration ranging from 14 % to 33 % (v/v) according to previous research [40]. Accordingly, the model gas used in this study contained 15 % CO_2, a water vapor pressure of 7 kPa. For this moisture content, a temperature of 50 °C before entering the oven in which the reactor is placed was chosen to avoid condensation in the gas line. The total gas flow rate was set to 20 L/min, with the unit expressed under normal conditions (0 °C and 1×10^5 Pa), based on preliminary tests that identified this value as the best optimum to ensure a measurable CO_2 uptake without complete CO_2 consumption. This would limit the carbonation of RCA because CO_2 would be a limiting reagent. Conversely, a higher flow rate would result in an outlet CO_2 flow rate very close to the inlet CO_2 flow rate, making accurate CO_2 uptake measurements more difficult due to sensor precision.

The schematic diagram of the setup is shown in Fig. 3 and a picture is presented in Fig. 4(a). Compressed air is supplied from the laboratory compressed air network, while CO_2 is provided from a bottle. The air first passes through a Shako UCFR-02 filter regulator, which retains moisture and any particles, and regulates the pressure to 2×10^5 Pa. This pressure is required for the proper operation of the Brooks Instrument SLA5800 Series mass flow controller, which is calibrated for air and positioned downstream of the filter.

After the mass flow controller, the air flow is split into two branches. Each branch passes through a Sho-Rate float flowmeter (Brooks Instrument). These float flowmeters are used solely to manually adjust and balance the flow between the two branches. A part of the air flow passes through a pipe immersed in a heated oil bath at 70 °C, while the other part is directed through a 1-liter bubbler filled with demineralized water, also immersed in the same oil bath. The two gas streams are then mixed in a static mixer. The humid air is then mixed with pure CO_2, which has been depressurized and whose flow rate is regulated by a Brooks Instrument SLA5800 Series mass flow controller. After regulation, the CO_2 is heated first in a pipe also immersed in the heated oil bath. The humid air and CO_2 are combined in a static mixer, and the resulting gas mixture is then directed toward the reactor. To prevent water condensation in downstream pipes, all pipes leaving the heated bath are fitted with a trace heating system and are insulated to improve thermal efficiency.

2.3. Carbonation procedure

Before each test, a 2.5 kg batch of RCA was conditioned to the target water saturation degree and placed in a closed plastic bag. Both the bag containing the RCA and the reactor were placed inside an oven at the test temperature for 4 h to ensure thermal equilibration prior to testing. The inlet gas preparation was switched on 1 h before the experiment to allow stabilization. The gas characteristics were then measured using the procedure described in Sections 2–4. The so-obtained values were considered representative of the gas conditions at the reactor inlet during carbonation.

The tested RCA samples was placed in the sealed cylindrical reactor (Ø200 mm diameter × 154 mm height) inserted in the oven (Fig. 4(b)). A mesh (80 µm) at the bottom allowed gas flow while preventing particle obstruction. The RCA bed (~7 cm high) was placed on the mesh. The RCA bed is much higher than the maximum particle diameter (4 mm), which ensures that the bed is sufficiently thick to be representative to the particle size distribution. The carbonation exposure was set to 120 min to maintain a relatively short process while ensuring a significant progression of the reaction. Gas flows through the RCA sample from the bottom to the top of the reactor. At the end of the test, the reactor was disconnected, and the gas composition was verified. The sample was weighed then oven-dried at 60 °C ($m_{60°C}$) until mass stabilization (mass variation < 0.05 %/24 h) to determine the final water content. Subsequently, the sample was quartered: 500 g were analyzed by Macro-TGA (Sections 2–6) and 250 g were used for water absorption tests (Sections 2–7).

2.4. Indirect monitoring of carbonation

Carbonation was monitored by measuring the drop in CO_2 molar flow between the reactor inlet and outlet (Fig. 5(a)). The inlet gas, considered stable, was analyzed before and after the test, while the outlet gas was analyzed continuously during the experiment (Fig. 3). CO_2 molar flow was determined by measuring CO_2 concentration with the GMP251 probe (Vaisala), and temperature (T_2) and pressure (P_2) with a LEO5 sensor (Keller). To ensure proper operation of the CO_2 level probe, which functions optimally below 60 °C, the gas was passed through a 40 cm glass condenser to lower its temperature and remove water vapor by condensation.

The molar flow rate of CO_2 was calculated using the measured CO_2 concentration, gas temperature, pressure, and humidity. The ideal gas law was used to convert the volumetric flow rate to molar flow rate.

The evolution of the quantity of CO_2 bound during the process, $n_{CO_2}^{uptake}$ [mol], was calculated by integrating the differences between the inlet and outlet CO_2 molar flow. At the end of the test, the final quantity of bound CO_2 is named $n_{CO_2}^{uptake,f}$ [mol]. The mass of bound CO_2, determined by the indirect method, is noted $G_{CO_2}^{indir}$ [g/kg$_{950°C}$] and is calculated as:

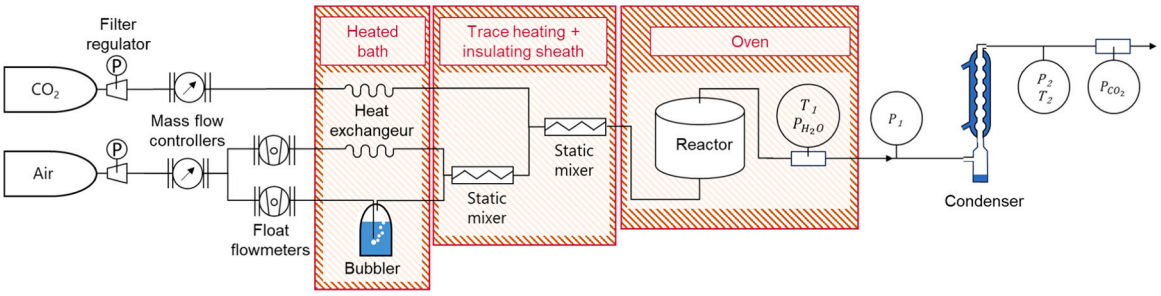

Fig. 3. Schematic diagram of the experimental setup, including the gas preparation system, the fixed-bed carbonation reactor and the gas analysis unit.

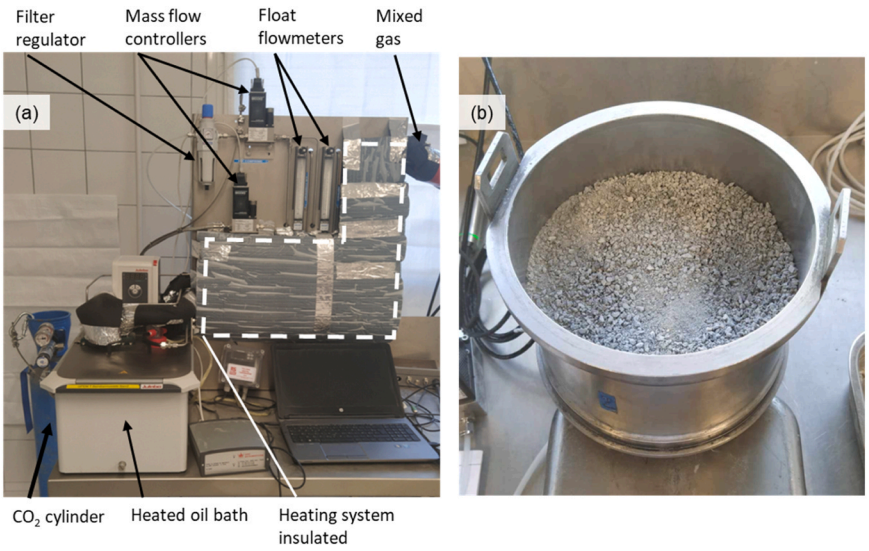

Fig. 4. Images of (a) the gas preparation station and (b) the fixed-bed reactor filled with RCA sample.

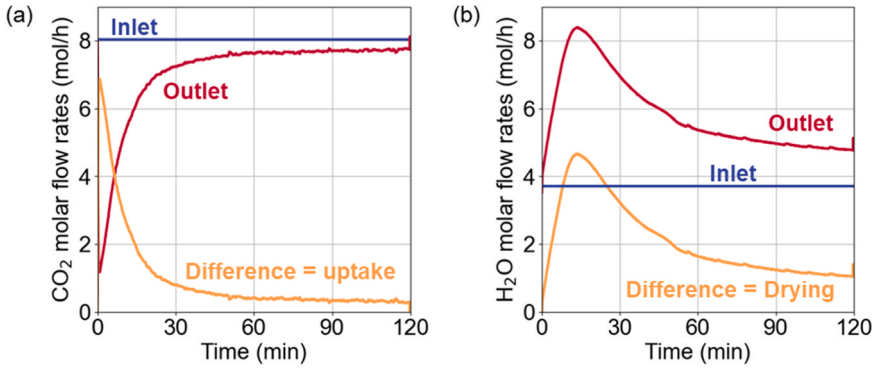

Fig. 5. Example of the evolution of flow rates of (a) CO_2 and (b) H_2O during a carbonation test at 50 °C for an initial water saturation degree of 0.93.

$$G_{CO_2}^{indir} = \frac{n_{CO_2}^{uptake} M_{CO_2} R_{60°C/950°C}}{m_{60°C}^{f}} \quad (3)$$

The amount of bound CO_2 within the material is expressed in grams per kilogram of material heated to 950 °C. This mass serves as a reference value, as it remains stable regardless of carbonation and moisture exchange with the environment.

2.5. Evolution of water saturation degree

Water flow at the reactor outlet was determined by measuring the gas temperature (T_1) and partial water pressure with a probe Vaisala HMP7, and the pressure (P_1) with a probe LEO2 (Keller) before the cooler. The total mass of water exchanged between the RCA and the gas ($m_{H_2O}^{exchange}$ [g]) was calculated by integrating the differences between incoming and outgoing water flows (Fig. 5(b)).

The mass balance of the water in the sample gives:

$$m_{H_2O}^{exchange,f} = m_{H_2O}^{i} - m_{H_2O}^{f} + m_{H_2O}^{carbo,f} \quad (4)$$

where $m_{H_2O}^{i}$ [g] and $m_{H_2O}^{f}$ [g] are the initial and final masses of water in the sample, determined from the water content of the sample before and after carbonation, respectively. $m_{H_2O}^{exchange,f}$ [g] is the final mass of water added to the gas throughout the experiment by exchange with the RCA. $m_{H_2O}^{carbo,f}$ [g] is the final mass of water produced during the carbonation reaction from the dehydroxylation of portlandite and the dehydration of hydrates. This value can be deduced from Eq. (3). The carbonation of certain hydrates, such as C-S-H, does not necessarily produce water [41]. As a result, the evolution of water production during the reaction $m_{H_2O}^{carbo,f}$ [g] is difficult to assess precisely but it is reasonable to assume that production of water during carbonation is proportional to the progress of the reaction. From this assumption, the evolution of water content is calculated as follows:

$$w = \frac{m_{H_2O}^{i} - m_{H_2O}^{exchange} + \zeta m_{H_2O}^{carbo,f}}{m_{60°C}^{i}} \times 100 \quad (5)$$

where ζ, between 0 and 1, represents the fraction of CO_2 uptake achieved at a given time, relative to the final uptake, and is given by $n_{CO_2}^{uptake} / n_{CO_2}^{uptake,f}$, and $m_{60°C}^{i}$ is the initial mass of the sample dried at 60 °C equal to $m^i / \left(1 + \frac{w^i}{100}\right)$, with m^i [g] the initial mass of sample and w^i (%) its water content.

To estimate the evolution of the water saturation degree, the water absorption of the samples, A [%], is estimated to be proportional to the progression of carbonation:

$$A = A_0 + \zeta (A_f - A_0) \quad (6)$$

Where A_0 is the water absorption of the non-carbonated material and A_f is the water absorption of the sample after carbonation. Water absorption is determined with the protocol presented in Section 2.7

2.6. Macroscopic thermogravimetric analysis (Macro-TGA)

The Macro-TGA method is a thermogravimetric analysis technique that, unlike conventional TGA, allows the use of sample masses in the range of several hundred grams instead of a few tens of milligrams. This larger sample size ensures better representativity of the material studied, particularly when it is strongly heterogeneous. The method was investigated in a previous study [38] to assess its applicability for RCA carbonation analysis.

A 2.5 kg sample was first quartered to obtain a representative 500 g subsample (Fig. 1). This subsample was then sieved into different fractions: 0/0.2 mm, 0.2/0.5 mm, 0.5/1 mm, 1/2 mm and 2/4 mm. Each fraction was subsequently placed in an oven (CWF-BAL 12/21 from Carbolite, Fig. 6(a)), where its mass was measured after three specific temperatures: 415 °C, 475 °C, and 950 °C. To ensure stability, each sample was held at the target temperature for at least three hours before being cooled to 105 °C to allow weighing each fraction outside the oven (Fig. 6(b)). The choice of temperatures, especially 415 and 475 °C, was based on a preliminary study. Details of the latter are provided in Appendix B. At 475 °C, portlandite (CH) is fully decomposed, while calcium carbonate remains stable. The mass loss up to this temperature is therefore attributed to the dehydration of CH, allowing the CH content to be quantified without overlap.

From the mass measurements at these three temperatures, the portlandite content, c_{CH} [g/kg$_{950°C}$], calcium carbonate content, c_{CC} [g/kg$_{950°C}$], and CO_2 content, c_{CO_2} [g/kg$_{950°C}$], were determined for each fraction as follows:

$$c_{CH} = \frac{1000 \times (m_{415°C} - m_{475°C}) \times M_{CH}}{m_{950°C} \times M_{H_2O}} \tag{7}$$

$$c_{CC} = \frac{1000 \times (m_{475°C} - m_{950°C}) \times M_{CC}}{m_{950°C} \times M_{CO_2}} \tag{8}$$

$$c_{CO_2} = \frac{1000 \times (m_{475°C} - m_{950°C})}{m_{950°C}} \tag{9}$$

$m_{415°C}$ [g], $m_{475°C}$ [g] and $m_{950°C}$ [g] are the masses of a fraction at 415 °C, 475 °C and 950 °C, respectively, and M_{H_2O} [g/mol], M_{CO_2} [g/mol], M_{CH} [g/mol] and M_{CC} [g/mol] are the molar masses of H_2O, CO_2, portlandite and calcium carbonate respectively.

The overall CO_2 content of all the fractions, $c^{tot}_{CO_2}$ [g/kg$_{950°C}$] was determined by the weighted sum of CO_2 content of each fraction:

$$c^{tot}_{CO_2} = \sum_{fractions} c^{fraction}_{CO_2} \frac{m^{fraction}_{950°C}}{m^{tot}_{950°C}} \tag{10}$$

with $c^{fraction}_{CO_2}$ [g/kg$_{950°C}$] the CO_2 content of a fraction determined in Eq. (9), $m^{fraction}_{950°C}$ [g] the mass of the fraction measured at 950 °C and $m^{tot}_{950°C}$ [g] the sum of the masses of all fractions at 950 °C.

The mass of CO_2 bound by carbonation ($G^{Macro-TGA}_{CO_2}$ [g/kg$_{950°C}$]) is calculated by subtracting the CO_2 content of the non-carbonated ($c^{NC}_{CO_2}$ [g/kg$_{950°C}$]) from the CO_2 content after carbonation:

$$G^{Macro-TGA}_{CO_2} = \left(c_{CC} - c^{NC}_{CC}\right) \times M_{CO_2} \tag{11}$$

Macro-TGA also provided the mass ratio $m_{60°C}/m_{950°C}$=$R_{60°C/950°C}$ used for the determination of the water content of the quasi-saturated RCA as described in Section 2.1.

In this study, the carbonation degree (DC [%]) is determined from the measured CO_2 content of the carbonated RCA (c_{CO_2} [g/kg$_{950°C}$]), using the following relationship:

$$DC(\%) = \frac{c_{CO_2} - c^{NC}_{CO_2}}{c^{max}_{CO_2} - c^{NC}_{CO_2}} \times 100 \tag{12}$$

with $c^{max}_{CO_2}$ [g/kg$_{950°C}$] is the theoretical maximum content of CO_2 that can be bound by the material, calculated with the cement and mortar compositions. It was considered that all cement oxides CaO, MgO, Na_2O et K_2O can react with CO_2 except the part of CaO that has already reacted with SO_3 to form gypsum ($CaSO_4{\cdot}H_2O$) [42]. Thus, the theoretical CO_2 binding capacity is calculated as:

$$c^{max}_{CO_2} = 100\left(\frac{\%_{CaO}}{M_{CaO}} - \frac{\%_{SO_3}}{M_{SO_3}} + \frac{\%_{MgO}}{M_{MgO}} + \frac{\%_{Na_2O}}{M_{Na_2O}} + \frac{\%_{K_2O}}{M_{K_2O}}\right) \frac{m_{cement} M_{CO_2}}{\frac{m_{cement}}{1+LOI/100} + m_{sand}} \tag{13}$$

where $\%_{CaO}$, $\%_{SO_3}$, $\%_{MgO}$, $\%_{Na_2O}$ and $\%_{K_2O}$ are the elemental mass concentrations [%] of SO_3, MgO, Na_2O and K_2O in cement according to its composition (Table 1). m_{cement} and m_{sand} are the masses of dry cement and sand and LOI [%] is the loss on ignition at 950 °C. For our mortar, $c^{max}_{CO_2}$ was therefore estimated to be of 158.7 g/kg$_{950°C}$.

2.7. Measurement of water absorption

The water absorption was assessed using an evaporimetry-based method adapted from Gentilini et al. [43] and Mechling et al. [44]. This approach allows for the identification of the "Saturated Surface Dry" (SSD) condition based on drying kinetics. RCA samples (250 g) were spread in a 5 mm-thick layer in a tray, covered with demineralized water, and soaked for 24 h. The sample was agitated during immersion to remove trapped air. After soaking, excess surface water was carefully removed. Drying at 60 °C was then performed in an oven equipped by a balance (CWF-BAL 12/21 from Carbolite), that allows continuous monitoring of sample mass.

After reaching a stable mass during the drying process, the sample was transferred to an oven at 60 °C for an additional 24 h to ensure the removal of any remaining moisture. The drying rate was calculated by

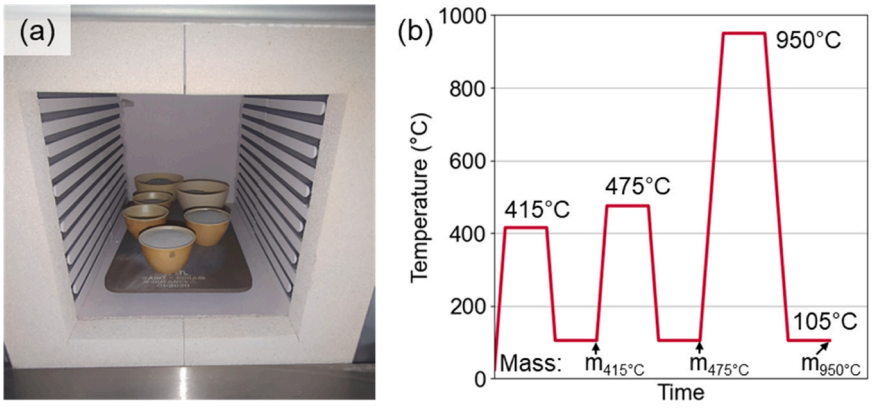

Fig. 6. (a) Picture showing the different fractions in the Macro-TGA; (b) the temperature program for the Macro-TGA.

deriving mass measurement over time. The evolution of the sample water content, w (%), was computed relative to the dry mass at 60 °C.

The water absorption, A (%), was then determined from the drying rate as a function of water content (Fig. 7). The SSD point was determined from the transition in drying rate between inter-particle and intra-particle water evaporation, the former being characterized by a constant drying rate [43,44]. It was identified as the water content at the intersection of the tangents corresponding to the two distinct drying phases. These tangents were calculated using a Python script applied to user-defined, yet clearly distinguishable, linear portions of the drying curve. The water absorption determined by this method corresponds to a reference mass at 60 °C.

3. Results

3.1. Initial material

Macro-TGA analysis was carried out for the five grain size classes of the non-carbonated material (Fig. 8(a)). Finer fractions (0/0.2 and 0.2/05 mm) contain higher portlandite and carbonate calcium due to their greater cement paste content. Cement paste is more friable than sand grains and tends to break down more easily during crushing [45]. The portlandite content of the finest fraction (0/0.2 mm) is slightly lower than that of the 0.2/0.5 mm fraction. This may be due to a natural carbonation of the finest particles during grinding and sample preparation. Overall, calcium carbonate content tends to be higher than portlandite content the finer the fraction. This is due to the increased surface area available for natural carbonation during sample preparation.

The theoretical maximum CO_2 binding capacity of the whole 0/4 mm fraction determined as 158.7 g/kg$_{950°C}$ (in part 2.6) was distributed among the different particle size classes according to their cement paste fraction deduced from their portlandite and $CaCO_3$ content as:

$$c_{CO_2}^{\max,fraction} = \frac{c_{CH}^{fraction} \Big/ M_{CH} + c_{CC}^{fraction} \Big/ M_{CC}}{c_{CH}/M_{CH} + c_{CC}/M_{CC}} c_{CO_2}^{\max} \quad (14)$$

with $c_{CO_2}^{\max,fraction}$ [g/kg$_{950°C}$], the theoretical maximum CO_2 content of a fraction, $c_{CH}^{fraction}$ [g/kg$_{950°C}$], its portlandite content and $c_{CC}^{fraction}$ [g/kg$_{950°C}$], its $CaCO_3$ content. The CO_2 content of RCA-NC and the theoretical maximum CO_2 content of each fraction are given in Fig. 8(b).

The whole 0/4 mm fraction of the non-carbonated RCA contains 21.6 g/kg$_{950°C}$ of CO_2, originating from the limestone of the cement and a natural carbonation during the preparation of the RCA (curing, storage, crushing, and preparation of water content). Although preventive actions were taken to prevent natural carbonation, such as immersion in water during curing, storage in sealed plastic bags, and minimizing exposure to air, carbonation cannot be completely suppressed.

3.2. Comparison of the carbonation assessment methods

As it was described previously, two methods were used to determine the amount of CO_2 bound by the sample: an indirect measurement of CO_2 consumption by analyzing the outlet gas (Section 2.4) and Macro-TGA (Section 2.6). The comparison between results obtained by these two methods, shown in Fig. 9, reveals that the Macro-TGA method yields a lower CO_2 content compared to the indirect method. The difference in CO_2 uptake between the two methods can reach up to 10 g/kg$_{950°C}$.

The differences between the results of the two methods are due to their limitations and uncertainties inherent in each. The uncertainty of the Macro-TGA method, which operates in steps, is mainly influenced by the choice of the temperature separation between dehydration and carbonation (namely 475 °C). In addition, the indirect method depends on the accuracy of the measurement devices, such as the Vaisala CO_2 sensor (±1.3 %). The overall precision of the method is estimated at 10 %.

Despite some differences between the results of the two methods, they complement each other: the indirect method tracks in real-time the CO_2 uptake during the test, while Macro-TGA quantifies the bound CO_2 in different granular fractions.

3.3. Effect of temperature and initial water saturation degree on CO_2 uptake

The continuous monitoring of CO_2 concentration at the reactor outlet provided insights into the evolution of CO_2 uptake by the material (Fig. 10). The carbonation kinetic decreases over time in all experiments. The most efficient carbonation occurred at 80 °C with an initial water saturation degree (S_i) of 0.60, with the RCA sequestering 71.1 g/kg$_{950°C}$ of CO_2, corresponding to a carbonation degree of 52 %. Comparable carbonation degrees have been reported in semi-dry processes [37,46], under similar reaction times. Even higher carbonation degrees can be achieved using liquid-phase carbonation methods [36,47], although such processes generally require additional steps, such as RCA grinding and solid–liquid separation, which make them less straightforward to implement at scale.

The temperature effect was found to vary with the initial water

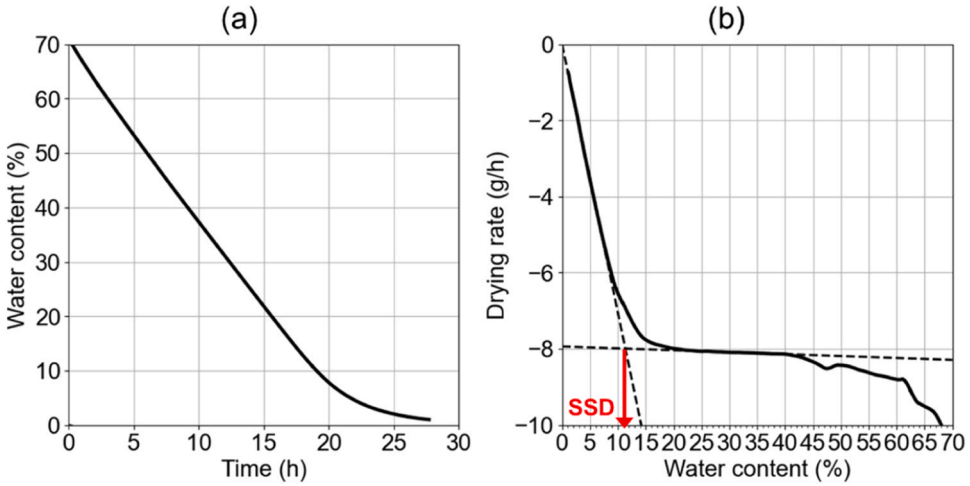

Fig. 7. Typical drying curve of RCA (carbonated at 110 °C with initial water saturation degree of 0.6) at 60 °C for the determination of the SSD point based on drying kinetics. (a) evolution of water content vs. time; (b) evolution of drying rate vs. the water content.

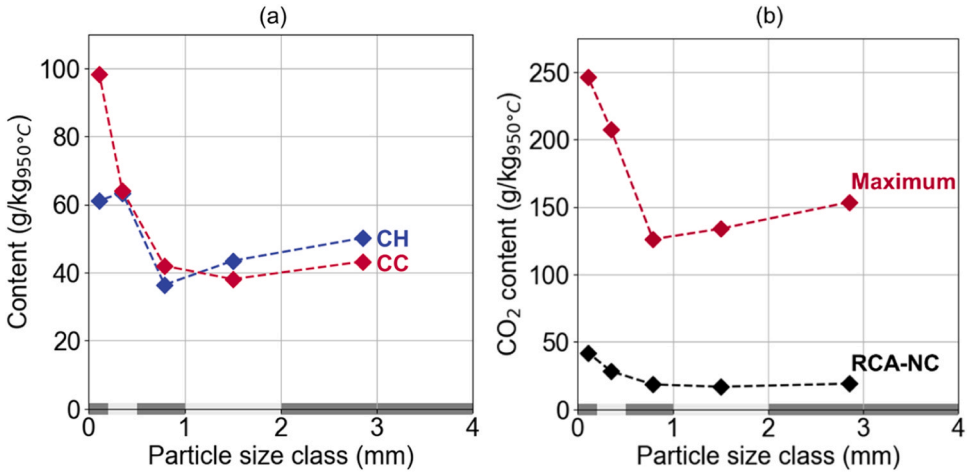

Fig. 8. (a) Portlandite (CH) and calcium carbonate (CC) contents determined by Macro-TGA for the non-carbonated recycled concrete aggregate (RCA-NC) for different particle size classes. (b) CO_2 content of the RCA-NC and the theoretical maximum as a function of the particle size class estimated from macro-TGA. Points are set at the median diameter (D_{50}) of the particle size class represented by the grey-shaded rectangles on the x-axis.

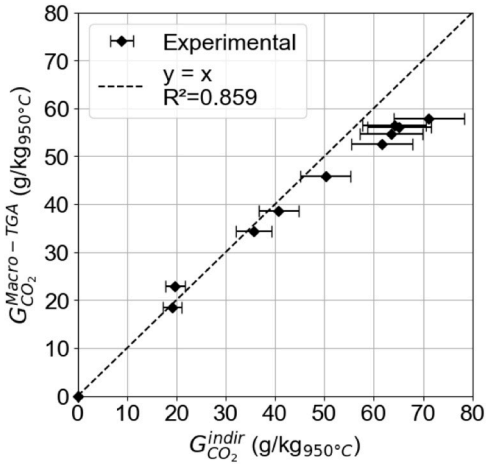

Fig. 9. Comparison between the CO_2 uptake obtained by Macro-TGA ($G_{CO_2}^{Macro-TGA}$) and the uptake calculated using the indirect method ($G_{CO_2}^{indir}$) for all tested conditions.

saturation degree of the RCA. When the initial water saturation degree was 0.34, carbonation efficiency decreased as temperature increased. In contrast, at an initial water saturation degree of approximately 0.93 (quasi-saturated material), carbonation was more efficient at 80 °C and 110 °C. For an initial water saturation degree of 0.60, the carbonation was maximal at 80 °C.

The least efficient test, performed at 110 °C with an initial water saturation degree of 0.34, was the only one where the carbonation kinetic became negligible after 90 min. It is likely that the sample did not contain enough water for carbonation to proceed further.

Studying the effect of temperature requires consideration of the material moisture state, which can change during the process. To account for this, we examined the changes in water saturation degree during the experiments. For this purpose, Fig. 11 illustrates the evolution of the average water saturation degree of the samples, determined by Eq. (1), which decreased throughout all experiments. This systematic decrease indicates that all experimental conditions—specifically, the vapor pressure of the inlet gas and the reactor temperature—favor the drying of the samples. The tests at 50 °C showed a slight initial increase in water saturation degree, likely due to the water produced by the carbonation process, which was faster than the drying of the RCA. It is worth noting that, overall, drying was faster than the water production by the reaction. This result suggests that water production via carbonation did not significantly counterbalance the drying effect.

For each initial water saturation degree of the samples, the water saturation degree decreased more rapidly at higher temperatures because increasing temperature both accelerated moisture exchange kinetics and reduced the effective relative humidity of the surrounding gas. The inlet gas had a constant water vapor pressure of 7 kPa, which corresponds to relative humidities of about 57 % at 50 °C and 15 % at 80

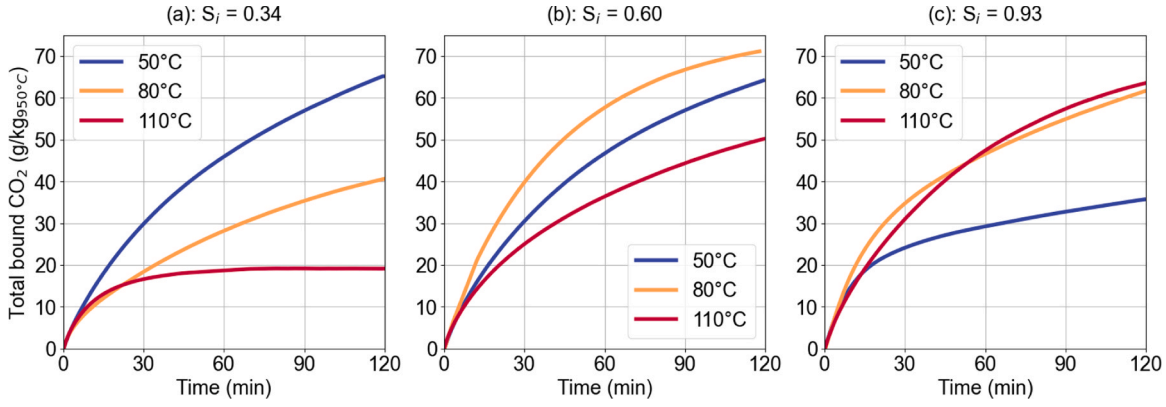

Fig. 10. Evolution of the total bound CO_2 on the entire fraction (0/4 mm), determined using the indirect method, at three temperatures, for initial water saturation degree of 0.34 (a), 0.60 (b) and 0.93 (c).

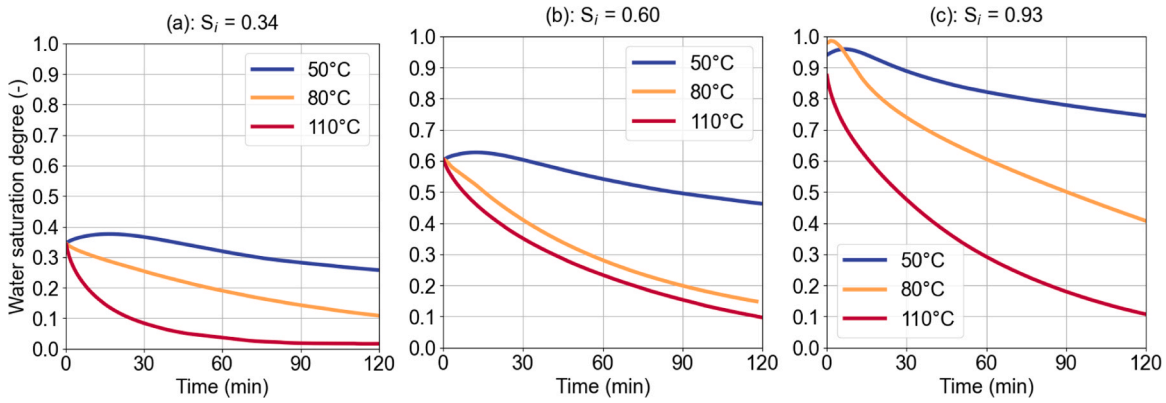

Fig. 11. Evolution of the average water saturation degree of the sample, at three temperatures, for initial water saturation degree of 0.34 (a), 0.60 (b), and 0.93 (c).

°C when expressed at the reactor temperature, assuming no interaction with the material. Above 100 °C, relative humidity cannot be defined under atmospheric pressure since no saturation vapor pressure exists. Consequently, higher temperatures simultaneously increase the driving force for water desorption and the rate of mass transfer, leading to faster drying of the RCA.

When removing the carbonated RCA samples with an initial water saturation degree of 0.93 at 50 °C from the reactor, we observed that the aggregates formed cohesive clumps. Although the final measured water saturation degree was 0.74, the cohesion observed suggests that residual water was still present on the surface or in the intergranular spaces of the RCA. This observation implies that the desorbed water did not completely migrate to the gas flow but remained locally trapped around the grains. Consequently, the water saturation degrees estimated earlier in the study are average water saturation degrees within the RCA bed, without specifying whether the water was in the aggregate pores or between the grains. Moreover, the measure does not imply an identical water distribution within the sample. An alternative explanation could be that cohesive clumps also result from partial binding between neighboring RCA particles, promoted by the precipitation of calcium carbonate at their contact surfaces. However, this effect appears less likely in the present case, as the clumps were no longer visible after drying, suggesting that water-induced cohesion was the dominant mechanism.

To better observe the combined effects of temperature (Fig. 10) and water saturation degree (Fig. 11), we plotted the cumulative CO_2 uptake over time as a function of the average water saturation degree of the samples for the three temperatures in Fig. 12.

At 15 min, carbonation appears to be slightly more efficient in samples with higher water saturation degree. Although samples carbonated at 80 °C fix slightly more CO_2, the effect of temperature remained limited during this early stage of process. At this point, carbonation likely occurs primarily at the surface of the grains, where reactive phases are directly accessible. A higher water saturation degree may slightly further facilitate the dissolution of reactive species on the surface, enhancing initial carbonation without requiring CO_2 to penetrate inside the grain.

As carbonation continues, the CO_2 uptake curve takes on a bell shape. After 60 min, the optimal water saturation degree for carbonation seems to be between 0.3 and 0.55 at 50 °C, around 0.3 at 80 °C, and above 0.3 at 110 °C. Furthermore, the impact of water saturation degree on carbonation becomes more pronounced, with the optimal water saturation degree decreasing as the reaction progresses. After 2 h, the optimal water saturation degree for the tests at 80 °C is found to be 0.15.

As the carbonation reaction advances, it occurs deeper within the grains, and the process becomes more influenced by the diffusion of CO_2 into the material. A higher water saturation degree hampers the diffusion process, slowing down the reaction. Therefore, as the reaction proceeds, the optimal water saturation degree decreases.

These observations highlight the critical influence of temperature on the drying behavior of samples during the carbonation process. Elevated temperatures accelerate water evaporation, modifying the internal moisture distribution and thereby impacting the local conditions for carbonation. While such drying can be beneficial for initially saturated samples by bringing their water saturation degree closer to optimal levels for the reaction, it can also have a detrimental effect on samples with low initial moisture, as excessive drying may hinder the dissolution of reactive species essential for effective carbonation.

Other studies have also highlighted the existence of an optimum water saturation degree to maximize carbonation [6,21]. Sereng et al. observed a maximum degree of carbonation for size 12/20 mm RCA

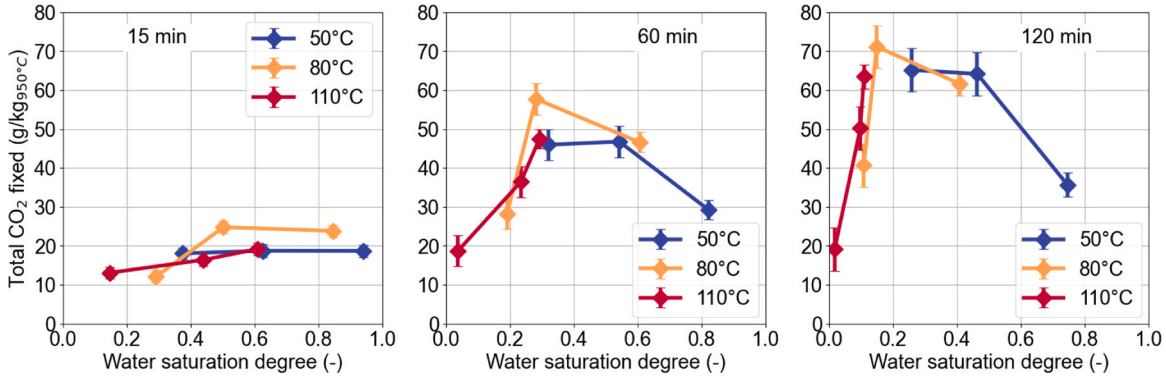

Fig. 12. Changes in cumulative amount of bound CO_2 determined by the indirect method as a function of the average water saturation degree of RCA bed at 15, 60, and 120 min and for three different temperatures. Lines are drawn to guide the eye but do not represent actual data points or values.

exposed for 24 h to an atmosphere containing 15 % CO_2, at 20 °C and 40 °C. This optimum carbonation was achieved when the water saturation degree of the RCA was 0.8. In our tests, the optimum water saturation degree appears to be between 0.15 and 0.45. However, several parameters vary between the two studies, such as aggregate size and carbonation time.

These results can serve to optimize an industrial system. The temperature in the reactor could be adjusted according to the initial water saturation degree of the RCA by adjusting the supply of hot gases emitted by industry.

3.4. Effect of the particle size on CO_2 uptake

To analyze the distribution of CO_2 uptake according to the grain size, we carried out Macro-TGA measurements on the different particle size classes obtained by screening after two hours of carbonation. The results are presented in Fig. 13, where data points correspond to the middle of the following size classes: 0/0.2 mm, 0.2/0.5 mm, 0.5/1 mm, 1/2 mm, and 2/4 mm.

For all tested conditions, the carbonation degree was consistently higher in finer fractions. At a given initial water saturation degree, the carbonation profiles across grain size classes exhibited similar shapes regardless of the temperature, with a vertical shift, suggesting that temperature affects the overall carbonation degree without altering the relative contribution of each size class.

Interestingly, the difference in carbonation degree between the finest (0–0.2 mm) and the coarsest (2–4 mm) fractions increases with higher initial water saturation degree. This difference ranged from 13 % to 23 % for S_i= 0.34, 25–33 % for S_i= 0.60 and 39–45 % for S_i= 0.93. This highlights the growing influence of CO_2 diffusion limitations as water saturation degree rises, particularly affecting the larger particles where carbonation is less pronounced. This trend supports the hypothesis that higher moisture hinders gas transport, restricting the carbonation front to the outer regions of coarse grains.

To help visualize the effect of carbonation parameters for each fraction, heatmaps for each fraction are plotted according to temperature and initial water saturation degree. The results (Fig. 14) indicate that the highest carbonation degrees follow a diagonal trend, increasing from the "cooler and drier" conditions to the "hotter and more water-saturated" ones. Optimal carbonation occurs when the initial water saturation degree and temperature provide sufficient moisture to dissolve reactive phases while not excessively hindering CO_2 diffusion.

For finer fractions (e.g., 0/0.2 mm), the carbonation degree is particularly high in samples with high initial water saturation degree. Although gas diffusion is more limited under high water saturation degree, the reduced particle size mitigates this effect. For instance, the highest carbonation degree for the 0.2–0.5 mm fraction occurs at 80 °C with S_i = 0.60 and 0.93, while for the 0–0.2 mm fraction, the maximum is observed at 80 °C and S_i = 0.93. This shift suggests that, as particle size decreases, the optimal water saturation degree for carbonation increases.

Conversely, for coarser fractions, carbonation decreases more significantly at S_i = 0.93. Larger particles experience greater CO_2 diffusion limitations, which become more pronounced at higher initial water saturation degrees. As a result, the influence of grain size on carbonation degree is most noticeable when water saturation degree is high. For the 1–2 mm and 2–4 mm fractions, the optimal conditions are 80 °C and S_i = 0.60.

The results presented in Fig. 15 clearly confirm that carbonation is highly dependent on particle size, with smaller fractions exhibiting significantly higher carbonation degrees. After both 15 and 120 min, the carbonation degree decreases consistently from 0 to 0.2 mm to 2–4 mm, confirming that CO_2 diffusivity through the porous grain is the main limiting factor of carbonation, as also emphasized in the Papadakis model [17]. The finest fraction (0/0.2 mm) is rapidly carbonated up to 49 % in 15 min while the coarsest fraction (2/4 mm) has a carbonation degree of only 6 %. This trend confirms the preferential carbonation of surface-accessible areas in the early stages, and the reduced efficiency of CO_2 penetration into larger particles over time.

3.5. Water absorption

The effect of carbonation on water absorption was assessed by comparing the water absorption of RCA before and after carbonation under different conditions. Fig. 16 shows the evolution of water absorption and the amount of bound CO_2 for several carbonation conditions. Carbonation process reduces the water absorption of RCA under all conditions. However, this reduction remains relatively small overall. A slightly more significant decrease is observed for the combination of 80 °C and an initial water saturation degree of 0.93.

No clear correlation emerges between the total amount of bound CO_2 and the water absorption. Carbonation has been associated with a reduction of fines capillary porosity (smaller than 30 nm) and with an increase in coarser capillary porosity (larger than 30 nm) [48,49]. This dual effect on the pore network could explain why samples with a similar carbonation degree may exhibit different total porosity evolutions.

4. Discussion

First, let us recall that the process studied here uses RCA to sequester CO_2 from an industrial gas. Carbonated RCA are then used for construction, either for road layers or for concrete formulation. Two points of view can therefore be adopted when analysing the results presented

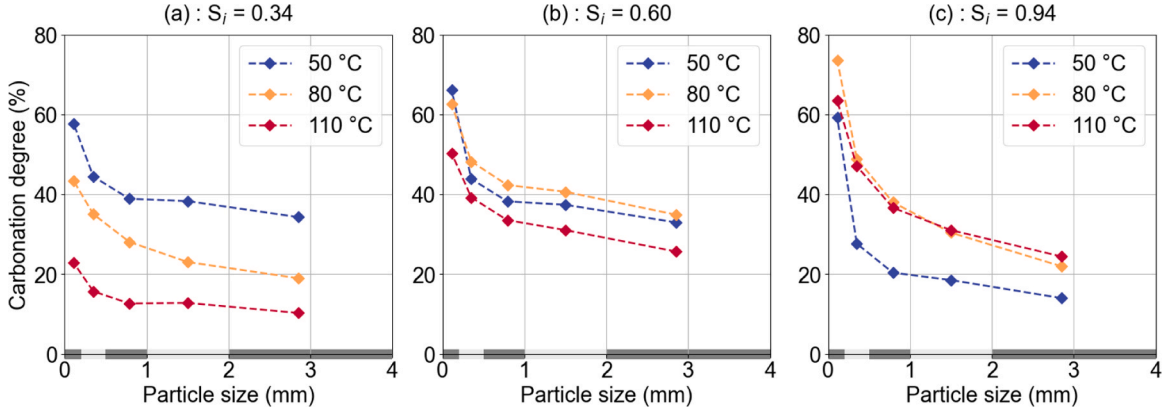

Fig. 13. Carbonation degree of the samples determined by Macro-TGA as a function of particle size fraction after 120 min of carbonation for different temperatures and initial water saturation degrees. Points are set at the median diameter (D_{50}) of the particle size class represented by the grey-shaded rectangles on the x-axis.

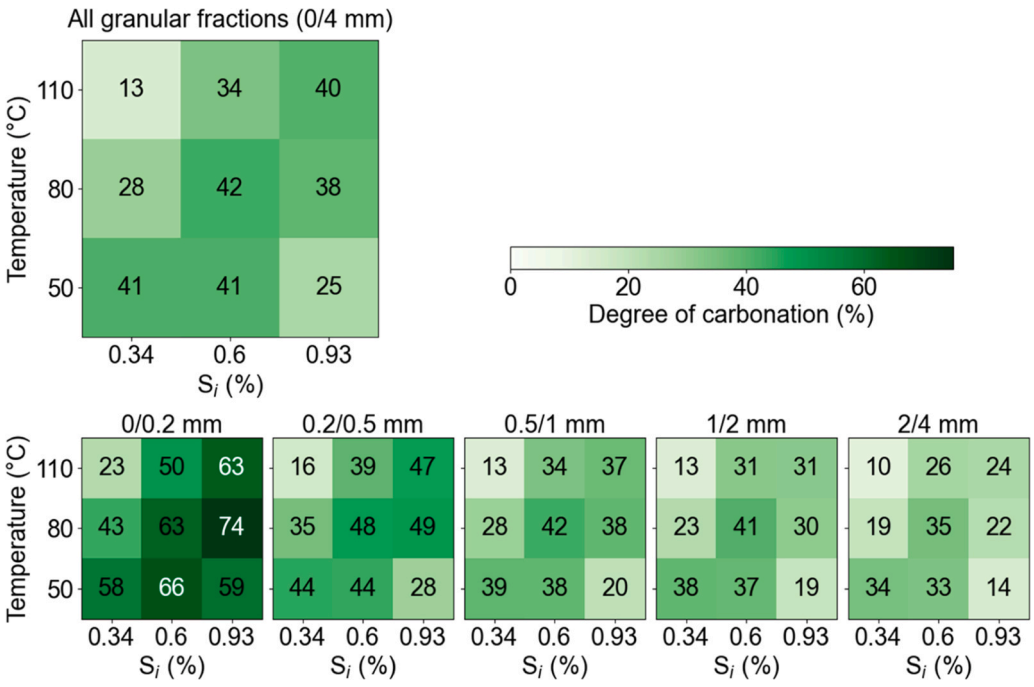

Fig. 14. Carbonation degree determined using Macro-TGA according to temperature and initial water saturation degree of RCA after 120 min of carbonation in the fixed-bed for each particle size fraction.

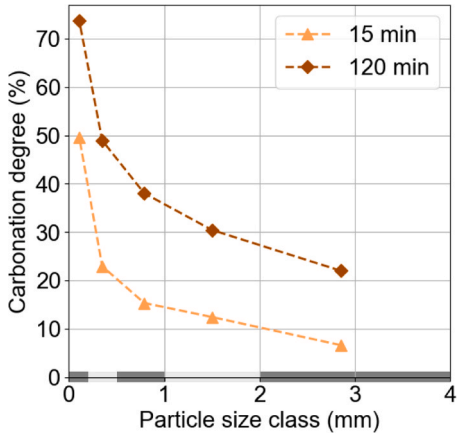

Fig. 15. Carbonation degree of the different granular size class carbonated at 80 °C with an initial water saturation degree of 0.93 after 15 min and 120 min exposure durations.

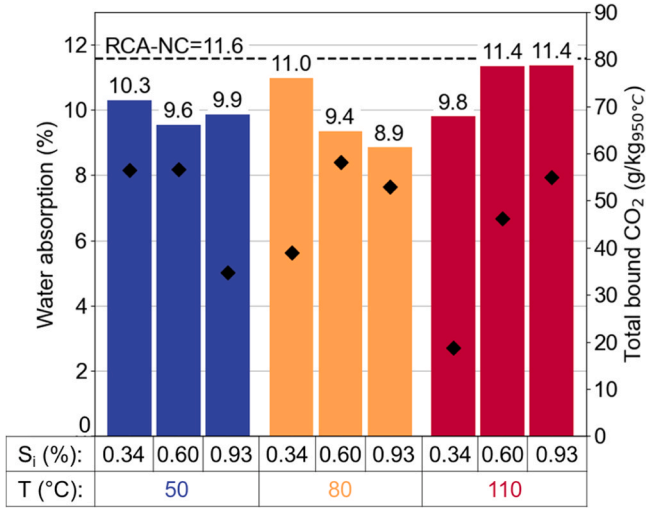

Fig. 16. Water absorption (bars, left axis) and bound CO_2 (scatter points, right axis) for several carbonation conditions (temperature and initial water saturation degree). The dotted horizontal line represents the water absorption of the non-carbonated RCA.

above: that of RCA production and that of CO_2 sequestration.

From the point of view of RCA production, the studied process applied for 2 h does not allow a significant improvement of the material since the water absorption coefficient is reduced by a maximum of only 23 %. We can deduce that the main interest of such a process is the capture and mineralisation of CO_2 and not the improvement of RCA. This is in line with the results of the FastCarb project using industrial-scale carbonators [10]. In this project, for instance, concretes made with RCA carbonated in a large-scale fluidized bed presented the same properties, especially compressive strength, as concretes containing non-carbonated RCA. It should be noted, however, that some studies have shown a higher reduction in water absorption after accelerated carbonation [6,42]. These studies used generally much longer carbonation duration with higher CO_2 concentrations.

Regarding CO_2 sequestration, the previous results can be analysed from the gas treatment efficiency, since the RCA bed can be considered as a gas filter. A filter instantaneous efficiency at a given time (t) [%] can be calculated as follows:

$$\eta(t) = 100\frac{F_{CO_2,in} - F_{CO_2,out}(t)}{F_{CO_2,\in}} \quad (15)$$

With: $F_{CO_2,in}$ the inlet CO_2 flowrate [mol.s^{-1}] and $F_{CO_2,out}$ the outlet CO_2 flowrate at time t [mol.s^{-1}].

Fig. 17 show the time-evolution of the so-calculated efficiency. The instantaneous efficiency at the beginning of the test exceeds 90 % at 80 °C for initial saturation degrees of 0.60 and 0.93. For all experiments, the initial instantaneous efficiency is higher than 70 %. However, efficiency decreases rapidly with time. After 30 min, the instantaneous efficiency falls below 40 % under all conditions. After 120 min, the highest instantaneous efficiency is observed at 50 °C with an initial

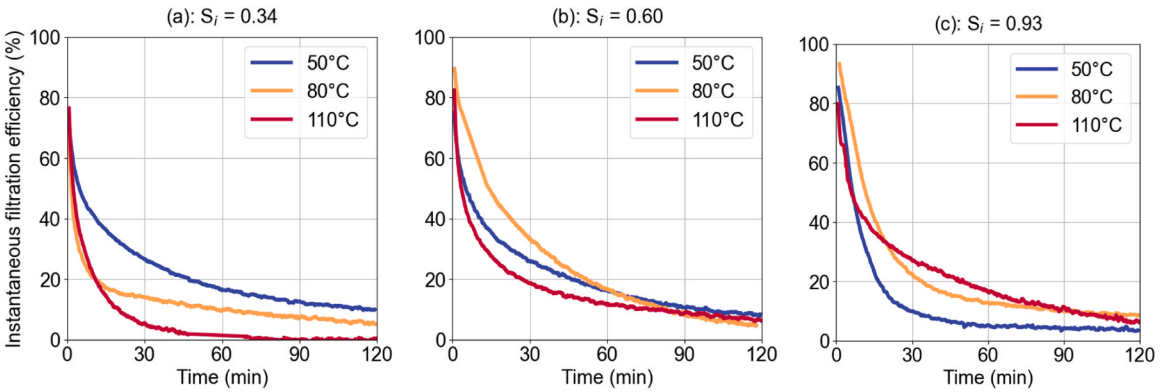

Fig. 17. Evolution of the instantaneous filter efficiency for the entire fraction (0/4 mm), determined using the indirect method, at three temperatures, for initial water saturation degree of 0.34 (a), 0.60 (b) and 0.93 (c).

saturation of 0.34, reaching approximately 10 %.

The cumulative filter efficiency up to the time t, $\bar{\eta}(t)$ [%], is calculated as follows:

$$\bar{\eta}(t) = 100\frac{n_{CO_2}^{uptake}(t)}{F_{CO_2,\in\times t}} \quad (16)$$

This calculation reveals that the RCA bed have bound between 5.8 % (110°C-Si=0.34) and 23.7 % (80°C-Si=0.60) of the CO_2 from the gas which has flowed through it for 2 h (Fig. 18 (a)). We note also that efficiency drops sharply during the first hour. Fig. 18 (b) shows also cumulative efficiency if we consider only the first hour.

The overall efficiency is also related to other operating parameter of the set-up, namely gas flow rate (20 L/min) and the height of the RCA bed (7 cm). Based on these two parameters, the contact time between the gas and the solid can be estimated at 2 s (assuming a porosity of 30 % for the bed). The reduction of the flow rate or the increase of the bed height would likely improve the filtration efficiency. However, such changes would also reduce the drying rate and affect the overall process performance, since the water saturation degree is a key parameter (Fig. 12). Moreover, these modifications would increase the CO_2 concentration gradient, leading to a non-uniform carbonation distribution along the bed. The effect of gas flow rate and bed height should therefore be explored in future studies.

Let us now examine our results in terms of large-scale application using an RCA bed as a flue gas filter. The water content of the RCA is undoubtedly the key-parameter of the process, as shown by (Fig. 12). This parameter is difficult to control because the aggregates are produced outdoors on crushing platform and can have a high-water content due to rain [7,50]. A pre-drying before carbonation is difficult to envisage because it would be energy-intensive. Our results show that the gas flow to be treated can it-self be used to dry the aggregates to a water saturation degree favourable for carbonation. One possible strategy could be to choose the gas temperature based on the water content of the RCA. The temperature could be set, for example, according to the sampling point in the chimney.

Another important factor to consider for large-scale implementation is the particle size distribution of the RCA. The efficiency of the filter could be improved by using finer particles than the 0/4 mm fraction used in this study. The finer particles, particularly below 500 µm, could further enhance the CO_2 capture efficiency by increasing the hydrates concentration in the reactor, increasing the specific surface area and improving gas–solid contact. Such an improvement could be achieved either by additional grinding or by sieving the RCA to retain only the finer fraction. Nevertheless, both options come with practical limitations. Additional grinding would increase the energy demand, which could offset part of the CO_2 captured during the process. On the other hand, selective sieving would reduce the available material and could complicate large-scale implementation. Moreover, since the finest fraction reacts more rapidly with atmospheric CO_2, it might already exhibit a high degree of natural carbonation before entering the accelerated carbonation process, thus reducing its effective capture potential. Note also that the goal of the studied process is to sequester CO_2 and produce RCA for construction. Grinding or sieving the used RCA would change the final product and its applications.

5. Conclusion

The objective of this study was to determine how temperature, initial water saturation degree, and RCA particle size influence carbonation efficiency in a fixed-bed crossed by a CO_2-rich gas flow simulating industrial flue gases from cement plants. Following conclusions can be drawn:

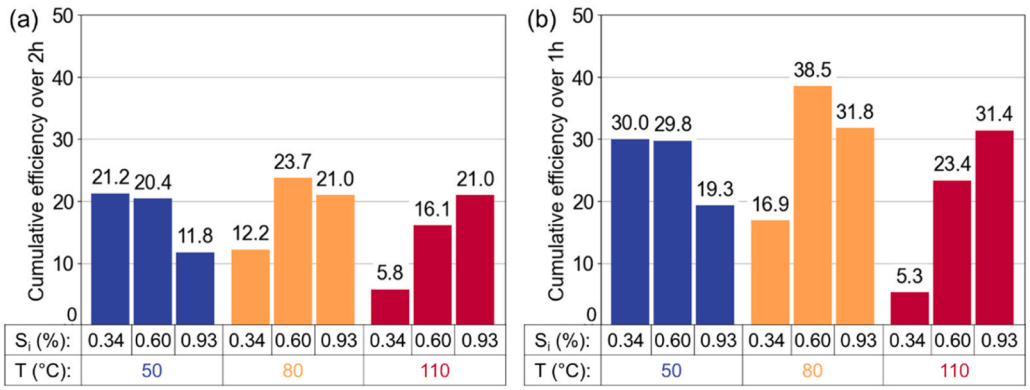

Fig. 18. Cumulative efficiency of the filter at the three temperatures and initial water saturation (a) over two hours and (b) over the first hour.

- An innovative thermogravimetric method (Macro-TGA) was used, enabling the analysis of up to 500 g of material instead of just a few milligrams. This approach enabled us to obtain more representative measurements of RCA carbonation.
- For each initial water saturation degree, an optimal temperature was highlighted for maximizing carbonation, achieving carbonation degrees exceeding 40 % within 2 h. While temperature alone has a limited effect on carbonation, it plays a crucial role in controlling moisture evolution throughout the process. Carbonation is most effective at temperatures that maintain a moderate water saturation degree, facilitating both gas transfer and RCA reactivity.
- Water saturation degree of RCA is a key factor in carbonation process, with an optimal moisture level balancing CO_2 diffusion and the availability of reactive hydrates. As carbonation progresses, the optimal water saturation degree shifts toward lower values. This suggests that while higher moisture levels initially promote the reaction, deeper carbonation within the RCA eventually requires more efficient CO_2 diffusion.
- Finer RCA fractions exhibit faster carbonation rates, and their optimal water saturation degree is higher compared to coarser fractions.
- Water absorption measurements before and after carbonation revealed a slight drop, with a maximum reduction of 2.7 % observed at 80 °C and initial water saturation degree of 0.93. No direct correlation was found between absorption reduction and carbonation degree, suggesting a more complex evolution of the pore structure that requires further investigation.
- The studied process is more effective at sequestering CO_2 than improving recycled aggregates.

Unlike most previous studies conducted on static samples, the present experiments were performed under dynamic gas flow through a granular bed, allowing a more realistic evaluation of the coupled effects of temperature and moisture on carbonation kinetics. Moreover, an important contribution of this study is the consideration of the evolving water saturation during carbonation. Unlike most previous works, which only considered initial water content of the materials or ambient relative humidity, we investigated the coupling between temperature and water content of the RCA throughout the test. This highlights that in a dynamic gas flow system, relative humidity alone does not fully describe the carbonation process and must be complemented by the material's water content and the surrounding temperature.

The insights gained from this study provide keys for optimizing carbonation parameters in industrial reactors. From an industrial perspective, the temperature of the inlet gas is a parameter that should be adjusted according to the water content of the RCA. Future research should focus on refining process conditions for large-scale applications and further characterize the homogeneity of the RCA bed and the microstructural changes induced by carbonation to better monitor its long-term effects on RCA properties.

Declaration of generative AI and AI-assisted technologies in the writing process

During the preparation of this work the authors used DeepL Write and ChatGPT-4 in order to improve the language and readability. After using these tools, the authors reviewed and edited the content as needed and take full responsibility for the content of the publication.

CRediT authorship contribution statement

ARTONI Riccardo: Writing – review & editing, Supervision, Methodology, Conceptualization. **TURCRY Philippe:** Writing – review & editing, Supervision, Methodology, Conceptualization. **AIT-MOKHTAR Abdelkarim:** Writing – review & editing, Project administration, Funding acquisition. **RICHARD Patrick:** Writing – review & editing, Funding acquisition. **CAZACLIU Bogdan:** Writing – review & editing, Methodology. **CORVEC Gaël:** Writing – original draft, Methodology, Investigation, Conceptualization.

Declaration of Competing Interest

The authors declare that they have no known competing financial interests or personal relationships that could have appeared to influence the work reported in this paper.

Acknowledgements

Funding for the CO_2NCRETE Project (ANR-20-CE05–0027) from the French National Research Agency (ANR) is gratefully acknowledged. We would like to thank everyone involved in the National Project FastCarb for their fruitful discussions.

Appendix A. Heat transfers in Macro-TGA

In thermogravimetric analysis, heat transfers can create thermal heterogeneity within the sample. To study this eventual problem, we estimated the characteristic thermal diffusion time, t_{diff} [s], defined as follows:

$t_{diff} \sim L^2/D$ with $L = H/2$ (half the 5 cm crucible height)

For typical mortar diffusivity $D = 5.10^{-7}$ $m^2.s^{-1}$ [51], t_{diff} is equal to 20 min. Each plateau in the stepwise macro-TGA described in Section 2.6 was maintained for at least 3 h, which is much higher than the characteristic thermal diffusion time. Thus, any thermal gradients were eliminated well before the mass readings were taken and the decomposition events of portlandite and $CaCO_3$ were reliably recorded. During the preliminary study described in Appendix B, the dynamic temperature ramp was set to 0.2 °C.min^{-1}. This implies a temperature difference of approximately 4°C between the center and border of the sample, that we consider negligible.

Appendix B. Choice of step temperatures

The choice of the three Macro-TGA step temperatures was based on a preliminary study conducted on both carbonated and non-carbonated RCA (0/4 mm). This study involved heating a sample at a slow temperature ramp of 0.2 °C/min from 300 °C to 950 °C in the balance-equipped furnace. This very slow temperature ramp is necessary to ensure the highest possible accuracy because it allows the sample to have a uniform temperature (see appendix B) and allows time for the species to decompose. The derivative of the mass loss curve was determined by local linear regression. The curves of thermal decomposition for the three RCA (Fig. A.1) indicate that portlandite decomposition begins after 415 °C. In non-carbonated RCA, the change in the derivative of the mass suggests that calcium carbonate ($CaCO_3$) decomposes beyond 560 °C. However, in carbonated RCA, $CaCO_3$ decomposition starts at 480 °C, overlapping with the decomposition range of portlandite. This decrease in $CaCO_3$ decomposition temperature is likely due to the formation, of less stable polymorphs than calcite, such as aragonite, vaterite, or amorphous forms [52]. Therefore, in stepwise thermogravimetric analysis, it is crucial to select appropriate temperatures between each decomposition step to accurately distinguish the mass losses associated with each phase. The temperature of 475 °C seems to enable portlandite decomposition without the decomposition of $CaCO_3$. Based on this preliminary

study, temperatures of 415 °C, 475 °C and 950 °C were chosen.

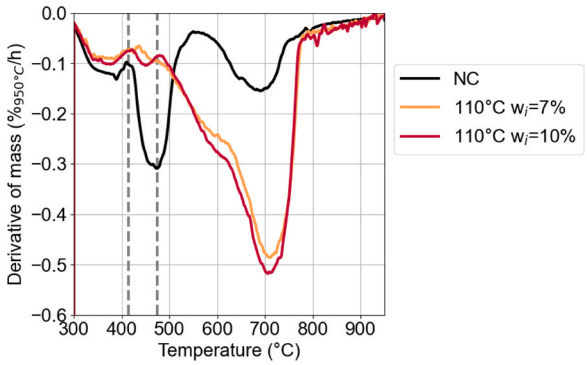

Fig. A.1. Evolution of the mass derivative for non-carbonated (NC) and carbonated (at 110 °C with initial water saturation degree of 0.6 and 0.93) RCA as a function of temperature. Vertical dashed lines are at 415 °C and 475 °C representing the two temperatures chosen for the temperature steps

Data availability

Data will be made available on request.

References

[1] L. Barcelo, J. Kline, G. Walenta, E. Gartner, Cement and carbon emissions, Mater. Struct. 47 (2014) 1055–1065, https://doi.org/10.1617/s11527-013-0114-5.

[2] Z. Cao, R.J. Myers, R.C. Lupton, H. Duan, R. Sacchi, N. Zhou, T. Reed Miller, J. M. Cullen, Q. Ge, G. Liu, The sponge effect and carbon emission mitigation potentials of the global cement cycle, Nat. Commun. 11 (2020) 3777, https://doi.org/10.1038/s41467-020-17583-w.

[3] K.-H. Yang, E.-A. Seo, S.-H. Tae, Carbonation and CO2 uptake of concrete, Environ. Impact Assess. Rev. 46 (2014) 43–52, https://doi.org/10.1016/j.eiar.2014.01.004.

[4] D. Zhang, CO2 utilization for concrete production: Commercial deployment and pathways to net-zero emissions, Sci. Total Environ. 931 (2024) 172753, https://doi.org/10.1016/j.scitotenv.2024.172753.

[5] Y. Villagran-Zaccardi, L. Ellwood, P. Perumal, J.M. Torrenti, Z. Zhao, E. Bernard, T. Hanein, T.C. Ling, W. Wang, Z. Zhang, R. Snellings, Carbonated recycled concrete aggregates in construction: potential and bottlenecks identified by RILEM TC 309-MCP, Mater. Struct. 58 (2025) 20, https://doi.org/10.1617/s11527-024-02489-6.

[6] M. Sereng, A. Djerbi, O.O. Metalssi, P. Dangla, J.-M. Torrenti, Improvement of Recycled Aggregates Properties by Means of CO2 Uptake, Appl. Sci. 11 (2021) 6571, https://doi.org/10.3390/app11146571.

[7] Y. Hou, P.-Y. Mahieux, P. Turcry, J. Lux, X. Jourdain, A. Aït-Mokhtar, Stockpile of recycled aggregates: A carbon sink, Constr. Build. Mater. 473 (2025) 140979, https://doi.org/10.1016/j.conbuildmat.2025.140979.

[8] M. Zajac, I. Maruyama, A. Iizuka, J. Skibsted, Enforced carbonation of cementitious materials, Cem. Concr. Res. 174 (2023) 107285, https://doi.org/10.1016/j.cemconres.2023.107285.

[9] S.A. Miller, G. Habert, R.J. Myers, J.T. Harvey, Achieving net zero greenhouse gas emissions in the cement industry via value chain mitigation strategies, One Earth 4 (2021) 1398–1411, https://doi.org/10.1016/j.oneear.2021.09.011.

[10] J.M. Torrenti, O. Amiri, L. Barnes-Davin, F. Bougrain, S. Braymand, B. Cazacliu, J. Colin, A. Cudeville, P. Dangla, A. Djerbi, M. Doutreleau, A. Feraille, M. Gueguen, X. Guillot, Y. Hou, L. Izoret, Y.-P. Jacob, J. Jeong, J.D.L. Hiu Hoong, P.-Y. Mahieux, J. Mai-Nhu, H. Martinez, V. Meyer, V. Morin, T. Pernin, J.-M. Potier, L. Poulizac, P. Rougeau, M. Saadé, L. Schmitt, T. Sedran, M. Sereng, A. Soive, G.S. Dos Reys, P. Turcry, The FastCarb project: Taking advantage of the accelerated carbonation of recycled concrete aggregates, Case Stud. Constr. Mater. 17 (2022) e01349, https://doi.org/10.1016/j.cscm.2022.e01349.

[11] S.M.N. Hassan, Techno-Economic Study of CO2 Capture Process for Cement Plants (Dissertation), University of Waterloo, 2005.

[12] D. Wang, J. Xiao, Z. Duan, Strategies to accelerate CO2 sequestration of cement-based materials and their application prospects, Constr. Build. Mater. 314 (2022) 125646, https://doi.org/10.1016/j.conbuildmat.2021.125646.

[13] M. Boumaaza, B. Huet, P. Turcry, A. Aït-Mokhtar, The CO2-binding capacity of synthetic anhydrous and hydrates: Validation of a test method based on the instantaneous reaction rate, Cem. Concr. Res. 135 (2020) 106113, https://doi.org/10.1016/j.cemconres.2020.106113.

[14] M. Boumaaza, B. Huet, G. Pham, P. Turcry, A. Aït-Mokhtar, C. Gehlen, A new test method to determine the gaseous oxygen diffusion coefficient of cement pastes as a function of hydration duration, microstructure, and relative humidity, Mater. Struct. 51 (2018) 51, https://doi.org/10.1617/s11527-018-1178-z.

[15] T. Chaussadent, État des lieux et réflexions sur la carbonatation du béton armé, Laboratoire central des ponts et chaussées, Paris, 1999.

[16] H. Mehdizadeh, Y. Wu, K.H. Mo, T.-C. Ling, Evaluation of carbonation conversion of recycled concrete fines using high-temperature CO2: Reaction kinetics and statistical method for parameters optimization, J. Environ. Chem. Eng. 11 (2023) 109796, https://doi.org/10.1016/j.jece.2023.109796.

[17] V.G. Papadakis, C.G. Vayenas, M.N. Fardis, Experimental investigation and mathematical modeling of the concrete carbonation problem, Chem. Eng. Sci. 46 (1991) 1333–1338, https://doi.org/10.1016/0009-2509(91)85060-b.

[18] I. Galan, C. Andrade, M. Castellote, Natural and accelerated CO2 binding kinetics in cement paste at different relative humidities, Cem. Concr. Res. 49 (2013) 21–28, https://doi.org/10.1016/j.cemconres.2013.03.009.

[19] E. Drouet, S. Poyet, P. Le Bescop, J.-M. Torrenti, X. Bourbon, Carbonation of hardened cement pastes: Influence of temperature, Cem. Concr. Res. 115 (2019) 445–459, https://doi.org/10.1016/j.cemconres.2018.09.019.

[20] D. Wang, T. Noguchi, T. Nozaki, Y. Higo, Investigation of the carbonation performance of cement-based materials under high temperatures, Constr. Build. Mater. 272 (2021) 121634, https://doi.org/10.1016/j.conbuildmat.2020.121634.

[21] E. Drouet, S. Poyet, J.-M. Torrenti, Temperature influence on water transport in hardened cement pastes, Cem. Concr. Res. 14 (2015).

[22] B.P. Hughes, I.R.G. Lowe, J. Walker, The diffusion of water in concrete at temperatures between 50 and 95C, Br. J. Appl. Phys. 17 (1966) 1545–1552, https://doi.org/10.1088/0508-3443/17/12/302.

[23] J.C. De Hemptinne, E. Behar, Propriétés thermodynamiques de systèmes contenant des gaz acides. Étude bibliographique, Oil Gas. Sci. Technol. 55 (2000) 617–637, https://doi.org/10.2516/ogst:2000047.

[24] F.P. Glasser, J. Pedersen, K. Goldthorpe, M. Atkins, Solubility reactions of cement components with NaCl solutions: I. Ca(OH) $_2$ and C-S-H, Adv. Cem. Res. 17 (2005) 57–64, https://doi.org/10.1680/adcr.2005.17.2.57.

[25] M. Jooss, H.W. Reinhardt, Permeability and diffusivity of concrete as function of temperature, Cem. Concr. Res. 32 (2002) 1497–1504, https://doi.org/10.1016/S0008-8846(02)00812-8.

[26] S. Omrani, M. Ghasemi, S. Mahmoodpour, A. Shafiei, B. Rostami, Insights from molecular dynamics on CO2 diffusion coefficient in saline water over a wide range of temperatures, pressures, and salinity: CO2 geological storage implications, J. Mol. Liq. 345 (2022) 117868, https://doi.org/10.1016/j.molliq.2021.117868.

[27] H. Peycelon, C. Blanc, C. Mazoin, Long-term behaviour of concrete: Influence of temperature and cement binders on the degradation (decalcification/hydrolysis) in saturated conditions, Rev. Eur. Génie Civ. 10 (2006) 1107–1125, https://doi.org/10.1080/17747120.2006.9692907.

[28] B. Coto, C. Martos, J.L. Peña, R. Rodríguez, G. Pastor, Effects in the solubility of CaCO3: Experimental study and model description, Fluid Phase Equilib. 324 (2012) 1–7, https://doi.org/10.1016/j.fluid.2012.03.020.

[29] B. Lu, S. Drissi, J. Liu, X. Hu, B. Song, C. Shi, Effect of temperature on CO2 curing, compressive strength and microstructure of cement paste, Cem. Concr. Res. 157 (2022) 106827, https://doi.org/10.1016/j.cemconres.2022.106827.

[30] Z. Lu, Q. Tan, J. Lin, D. Wang, Properties investigation of recycled aggregates and concrete modified by accelerated carbonation through increased temperature, Constr. Build. Mater. 341 (2022) 127813, https://doi.org/10.1016/j.conbuildmat.2022.127813.

[31] F. Kaddah, O. Amiri, P. Turcry, H. Ranaivomanana, E. Roziere, Coupled thermo-hydro-chemical modeling of accelerated carbonation of cement-based materials: application to CO2 uptake, J. Build. Eng. (2024) 109819, https://doi.org/10.1016/j.jobe.2024.109819.

[32] Q. Liu, H. Tang, K. Chen, C. Sun, W. Li, S. Jiao, V.W.Y. Tam, Improving industrial drying process of recycled fine aggregates as a means of carbonation to improve the mechanical properties and plastic shrinkage of self-leveling mortar, Constr. Build. Mater. 403 (2023) 133001, https://doi.org/10.1016/j.conbuildmat.2023.133001.

[33] L. Liu, J. Ha, T. Hashida, S. Teramura, Development of a CO2 solidification method for recycling autoclaved lightweight concrete waste, J. Mater. Sci. 4 (2001), https://doi.org/10.1023/A:1012591318077.

[34] Y. Wu, High-temperature CO2 for accelerating the carbonation of recycled concrete fines, J. Build. Eng. 11 (2022).

[35] Y. Mao, P. He, S. Drissi, J. Zhang, X. Hu, C. Shi, Effect of conditions on wet carbonation products of recycled cement paste powder, Cem. Concr. Compos 144 (2023) 105307, https://doi.org/10.1016/j.cemconcomp.2023.105307.

[36] M. Zajac, M. Król, F. Bullerjahn, J. Deja, Effect of temperature on carbon dioxide mineralisation in recycled cement paste, Adv. Cem. Res. 35 (2023) 384–395, https://doi.org/10.1680/jadcr.22.00129.
[37] D. Wang, T. Noguchi, M. Nanao, T. Nozaki, T. Hayakawa, Parametric investigation and scale testing on accelerated CO2 sequestration of cement-based materials by utilizing industrial waste heat, J. Clean. Prod. 475 (2024) 143716, https://doi.org/10.1016/j.jclepro.2024.143716.
[38] Y. Hou, P. Turcry, P.-Y. Mahieux, B. Cazacliu, J. Lux, A. Aït-Mokhtar, A comparative study of CO2 uptake quantification methods: A case study on recycled concrete aggregates under natural carbonation, J. Build. Eng. 101 (2025) 111845, https://doi.org/10.1016/j.jobe.2025.111845.
[39] A. Yacoub, A. Djerbi, T. Fen-Chong, The effect of the drying temperature on water porosity and gas permeability of recycled sand mortar, Constr. Build. Mater. 214 (2019) 677–684, https://doi.org/10.1016/j.conbuildmat.2019.04.128.
[40] A. Bosoaga, O. Masek, J.E. Oakey, CO2 Capture Technologies for Cement Industry, Energy Procedia 1 (2009) 133–140, https://doi.org/10.1016/j.egypro.2009.01.020.
[41] A. Morandeau, M. Thiéry, P. Dangla, Investigation of the carbonation mechanism of CH and C-S-H in terms of kinetics, microstructure changes and moisture properties, Cem. Concr. Res. 56 (2014) 153–170, https://doi.org/10.1016/j.cemconres.2013.11.015.
[42] B. Zhan, C.S. Poon, Q. Liu, S. Kou, C. Shi, Experimental study on CO2 curing for enhancement of recycled aggregate properties, Constr. Build. Mater. 67 (2014) 3–7, https://doi.org/10.1016/j.conbuildmat.2013.09.008.
[43] P. Gentilini, O. Yazoghli-Marzouk, V. Delmotte, Y. Descantes, Determination of the water content of fillerised fine aggregates in the saturated surface dry state, Constr. Build. Mater. 98 (2015) 662–670, https://doi.org/10.1016/j.conbuildmat.2015.08.131.
[44] J.-M. Mechling, A. Lecomte, K. Merriaux, Mesure de l'absorption d'eau des additions minérales des bétons par évaporométrie: Measurement of the absorption of water of the mineral admixtures in concrete by evaporometry, Mater. Struct. 36 (2003) 32–39, https://doi.org/10.1007/BF02481568.
[45] Z. Zhao, S. Remond, D. Damidot, W. Xu, Influence of hardened cement paste content on the water absorption of fine recycled concrete aggregates, J. Sustain. Cem. Based Mater. 2 (2013) 186–203, https://doi.org/10.1080/21650373.2013.812942.
[46] M. Zajac, J. Skibsted, F. Bullerjahn, J. Skocek, Semi-dry carbonation of recycled concrete paste, J. CO2 Util. 63 (2022) 102111, https://doi.org/10.1016/j.jcou.2022.102111.
[47] S. Liu, P. Shen, D. Xuan, L. Li, A. Sojobi, B. Zhan, C.S. Poon, A comparison of liquid-solid and gas-solid accelerated carbonation for enhancement of recycled concrete aggregate, Cem. Concr. Compos 118 (2021) 103988, https://doi.org/10.1016/j.cemconcomp.2021.103988.
[48] D.J. Anstice, C.L. Page, M.M. Page, The pore solution phase of carbonated cement pastes, Cem. Concr. Res. 35 (2005) 377–383, https://doi.org/10.1016/j.cemconres.2004.06.041.
[49] V.T. Ngala, C.L. Page, Effects of carbonation on pore structure and diffusinal properties of hydrated cement pastes, Cem. Concr. Res. 27 (1997) 995–1007, https://doi.org/10.1016/S0008-8846(97)00102-6.
[50] A. Leemann, B. Münch, M. Wyrzykowski, CO2 absorption of recycled concrete aggregates in natural conditions, Mater. Today Commun. 36 (2023) 106569, https://doi.org/10.1016/j.mtcomm.2023.106569.
[51] T.L. Bergman, A.S. Lavine. Fundamentals of heat and mass transfer, Eighth edition, John Wiley & Sons, Hoboken, NJ, 2017.
[52] M. Thiery, P. Dangla, P. Belin, G. Habert, N. Roussel, Carbonation kinetics of a bed of recycled concrete aggregates: A laboratory study on model materials, Cem. Concr. Res. 16 (2013).